Supporting Information

Krieger et al. 10.1073/pnas.1018887108

SI Materials and Methods.

Reagents. N-(4,4-difluoro-1,3,5,7-tetramethyl-4-bora-3a,4a-diaza-s-indacene-2-yl) iodoacetamide (BODIPY) and monobromobimane FluoroPure grade (mBBr) were purchased from Invitrogen. N-(Iodoacetaminoethyl)-1-naphthylamine-5-sulfonic acid (IAEDANS) and iodoacetamide (IAM) were purchased from Sigma.

Preparation of Ghosts. Fresh whole blood from 4.1R-null mice was shipped from the New York Blood Center together with WT blood, which was also sometimes purchased from Covance. Erythrocytes were segregated from whole blood by centrifugation and washed once with isotonic phosphate-buffered saline (PBS; 10 mM sodium phosphate, 150 mM potassium chloride, pH 7.4). Cells were then lysed in approximately 30 volumes hypotonic buffer (5 mM sodium phosphate, 5 mM potassium chloride, 2 mM magnesium chloride pH 7.4). White ghosts were washed with hypotonic buffer until hemoglobin was almost completely removed (approximately 5×) and resealed with isotonic buffer containing 200 μM IAEDANS (Sigma). Pink ghosts were not washed and were instead resealed immediately after lysis. Because the hemoglobin in pink ghosts would compete with spectrin for thiol label, pink ghosts were resealed in isotonic buffer containing 400 μM IAEDANS. The concentration of IAEDANS in pink ghosts was chosen so that the fluorescence intensity of spectrin matched the fluorescent intensity of spectrin in white ghosts loaded with 200 μM IAEDANS after static labeling. Both white and pink ghosts were resealed at room temperature for 30 min in the dark.

Labeling of Ghosts During Shear. Resealed ghosts were washed once in PBS, then resuspended in labeling solution containing 2 mM BODIPY 504/507 (Invitrogen) or for MS samples, mBBr (Invitrogen) in PBS. The suspension was divided into two samples. The static sample was covered in foil and incubated on a heat block at 37 °C, and the shear sample was loaded onto a temperature-controlled cone and plate rheometer set to 37 °C. Samples were then sheared at various stresses for up to 1 h, then washed once in ice-cold PBS. For kinetic mass spectrometry studies, ghosts were sheared for two time intervals, 30 and 60 min, where $t = 0$ designates the addition of the second dye. Previous Cys-labeling studies of RBC (1) have shown that 30 min of static labeling with IAEDANS is sufficient to saturate a large fraction of exposed Cys, establishing a baseline or background labeling. Additional shear labeling times were long enough to enhance the labeling above this background level.

SDS-PAGE Analysis. Ghosts prelabeled with IAEDANS, then labeled with BODIPY during shear were lysed with Radio-Immunoprecipitation Assay buffer containing 1% Triton-X 100 at 4 °C for 30 min, and lysates separated on 3–8% or 7% Tris-Acetate buffered polyacrylamide gels. Fluorescent images were taken immediately after the run was complete, and gels were stained with Coomasie R-250. Fluorescent and Coomassie intensities were measured using ImageJ. For wild-type red cells, lysates were run in multiple lanes with different loadings. Proteins were identified based on molecular weight. Fluorescent intensity versus Coomassie intensity plots were made for each band. If $R^2 < 0.9$, lysates were rerun on PAGE gels or experiments repeated. For most samples, $R^2 > 0.95$. Shear-enhanced labeling was calculated by the ratio of slopes of the sheared and static samples, with ratios > 1.1 considered shear-enhanced. All experiments with white ghosts were repeated at least twice, and error bars indicate the range of m_{shear}/m_{static} values at that shear stress. Experiments with pink ghosts were done once. Because of the scarcity of 4.1R-null sample, lystates were run in single lanes. Error bars are the estimated range of values based on the variation of 4.1R-null m_{static} values from three independent experiments. Fluorescent intensity was normalized by Coomassie intensity, and shear-enhanced labeling was calculated from the ratio of normalized shear : static fluorescent intensities.

Liquid Chromatography–Tandem Mass Spectrometry (LC-MS/MS) Analysis. For mass spectrometry analysis, ghosts were prelabeled with IAEDANS and then labeled with mBBr during shear. Lysates were made and separated as described above. Alpha and beta spectrin bands were excised for in-gel trypsin digest. Tryptic peptides were analyzed by LC-MS/MS on a LTQ-Orbitrap XL mass spectrometer (Thermo Fisher Scientific) interfaced with an Eksigent Autosampler/NanoLC-2D system (Eksigent Technologies). Peptides were eluted at 300 nL/min using an acetonitrile gradient consisting of 3–28% B over 40 min, 28–50% B over 25.5 min, 50–80% B over 5 min, 80% B for 5 min before returning to 3% B in 1 min. To minimize carryover, a blank cycle was run between each sample. The mass spectrometer was set to perform a full MS scan (m/z 350–2,000) in the Orbitrap, and the six most intense ions exceeding a minimum threshold of 1,000 were selected for MS/MS in the linear trap with dynamic exclusion enabled. Protein identification was done using the SEQUEST algorithm in BioWorks 3.3.1 (Thermo Fisher Scientific). Data were searched against a mouse database using a partial tryptic constraint with a 1.1 Da precursor mass tolerance, and allowing for methionine sulfoxide, IAM, IAEDANS, or mBBr cysteine modifications. Peptide identifications were filtered using the following criteria: mass tolerance ≤5 ppm, $\Delta Cn \geq 0.069$, and $Sf \geq 0.2$. The extent of IAEDANS, mBBr, and IAM labeling at each site was determined from extracted ion chromatograms with identification of each specific Cys achieved through both the m/z of the modified-Cys peptide as well as the MS/MS fragmentation pattern. Ion-flux values of Cys-labeled peptides from shear and static samples were normalized by their corresponding Cys-IAM ion-flux values. Phi values were calculated from the ratios of normalized shear and static ion fluxes, with phi > 1.25 defined as force-enhanced labeling. When multiple peptides were detected for the same cysteine, peptides with the greater ion-flux values were chosen to be represented in Fig. 5.

Sequence Alignment and Structure Predictions. Amino acids of alpha and beta spectrin were numbered according to UnitProt files P08032 and P15508, respectively. All alignments were done with ClustalW 2.0.12 (2). Solvent exposure of cysteines within repeat domains was estimated according to Parry et al. (3). Heptad position predicted was based on alignment with repeats 16–17 of chick nonerythrocytic spectrin, Protein Data Bank (PDB) ID code 1CUN. For Cys-β1159 position was based on alignment with repeats 8–9 in human erythrocytic spectrin, PDB ID code 1S35. For Cys-α129, the CH1 domain was aligned with human α-actinin 3, PDB ID code 3LUE. Cys-β1883 was aligned with repeats 14–15 of human spectrin, PDB ID code 3E57. Homology models for ankyrin cysteines Cys-274, Cys-316, and Cys-472 were aligned with the crystal structure of human ankyrinR repeat domains 13–24, PDB ID code 1N11. All homology models were generated by MODELLER 9v8 (4) based on ClustalW alignments. The coordinates of the mouse spectrin CH1 domain in reference to actin were determined using Chimera, based on the superposition of the homology model with the CH1 domain in PDB ID code

3LUE. All images of homology models were produced using Jmol.

Fluorescent Labeling of Fragments. Wild-type ghosts were loaded with BODIPY as described above, then incubated at 37 °C under 4 Pa shear stress or static conditions. Postthiol labeling, DiI, and glutathione (final concentration 10 mM) were added to the reaction solution and incubated for 20 min at room temperature to label membrane and quench excess dye.

Antibodies and Immunostaining. Anti-mouse CD47 antibodies were obtained from BD Biosciences (clone miap301). Secondary antibody used to detect CD47 was goat anti-rat IgG R-phycoerythrin purchased from Invitrogen. Post BODIPY labeling at 37 °C during 1.5 Pa shear and static conditions were incubated with CD47 antibody in PBS (1:500) for 20 min at room temperature. Ghosts were washed and incubated with secondary in PBS (1:1000) with DiI for 20 min at room temperature followed by washing and imaging on polylysine coated coverslips.

Fluorescent Imaging of Ghosts. For quantitative microscopy, ghosts were prelabeled with IAEDANS, then incubated with BODIPY and labeled under 1 or 2 Pa shear stress or static conditions. Fluorescent images of labeled ghosts were taken on an inverted microscope (IX71; Olympus) with a 60× (oil, 1.4 NA) objective using a Cascade CCD camera (Photometrics). Background subtraction and subsequent image analysis was done using ImageJ. Image acquisition was performed with Image Pro software (Media Cybernetics, Inc.) and results are shown in Fig 2*C*. Representative images from these experiments are displayed in Fig 1*C* as "0 Pa," "1 Pa," and "2 Pa." Ghosts BODIPY labeled during 1.5 Pa shear stress and immunostained for CD47 were imaged using a 150× (oil, 1.45 NA) objective. A side-view static-labeled ghost from this experiment appears in Fig S4*B*. Fragments were also imaged using the 150× objective.

1. Johnson CP, Tang HY, Carag C, Speicher DW, Discher DE (2007) Forced unfolding of proteins within cells. *Science* 317:663–666.
2. Thompson JD, Higgins DG, Gibson TJ (1994) CLUSTAL W: Improving the sensitivity of progressive multiple sequence alignment through sequence weighting, position-specific gap penalties and weight matrix choice. *Nucleic Acids Res* 22:4673–4680.
3. Parry DA, Dixon TW, Cohen C (1992) Analysis of the three-alpha-helix motif in the spectrin superfamily of proteins. *Biophys J* 61:858–867.
4. Sali A, Blundell TL (1993) Comparative protein modelling by satisfaction of spatial restraints. *J Mol Biol* 234:779–815.

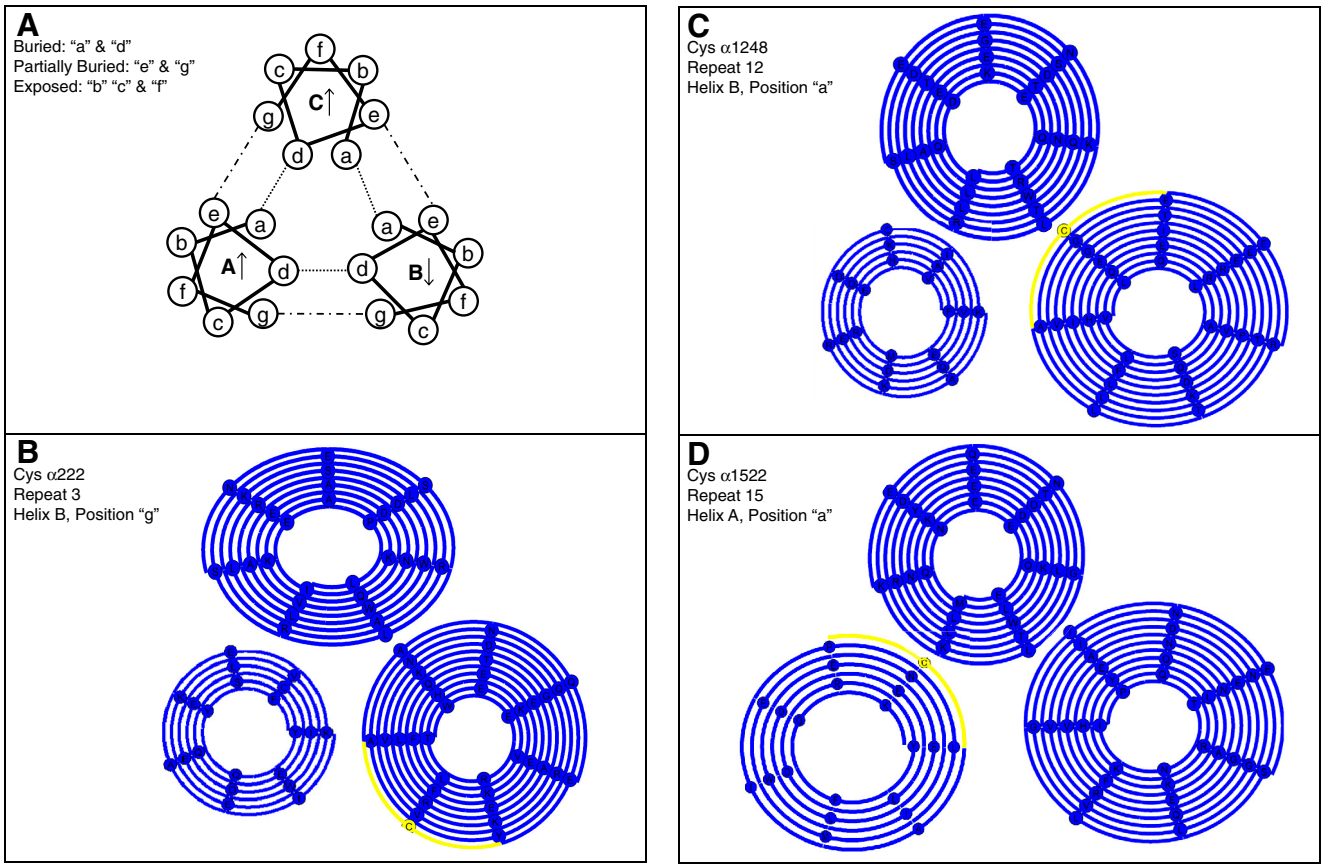

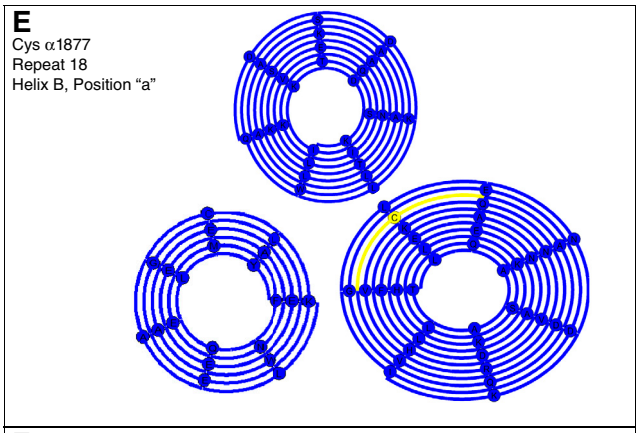
E
Cys α1877
Repeat 18
Helix B, Position "a"

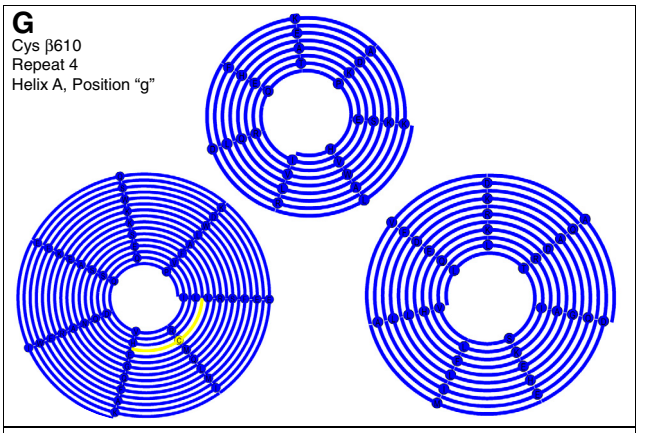
G
Cys β610
Repeat 4
Helix A, Position "g"

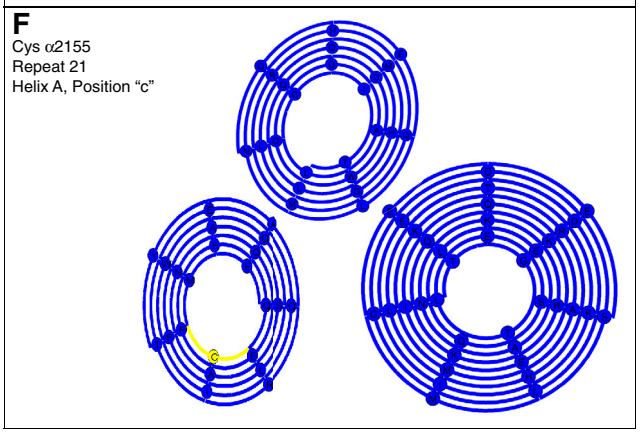
F
Cys α2155
Repeat 21
Helix A, Position "c"

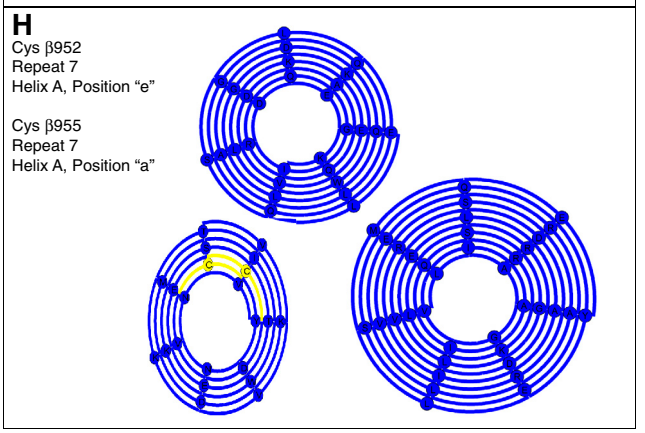
H
Cys β952
Repeat 7
Helix A, Position "e"
Cys β955
Repeat 7
Helix A, Position "a"

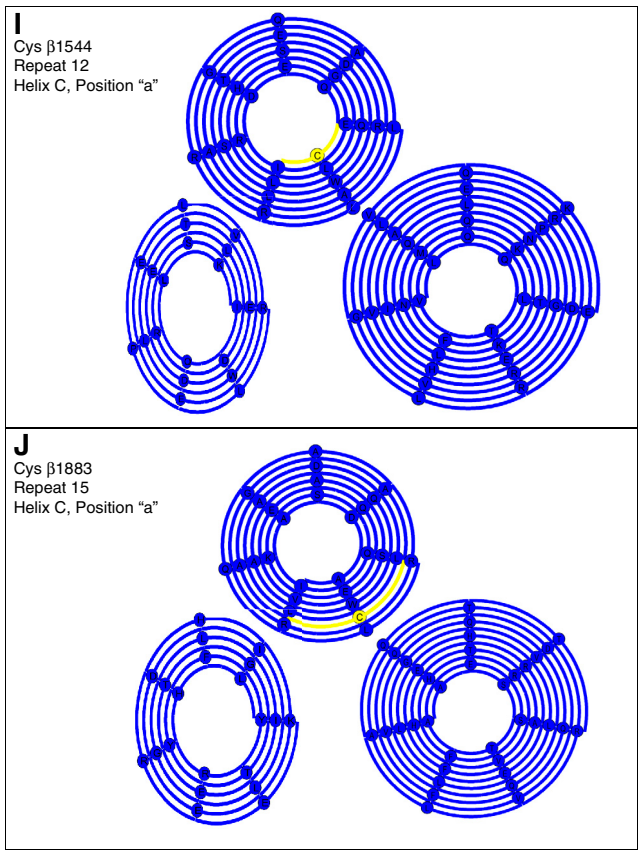

Fig. S1. Helical wheel depictions of repeat domains indicating hydrophobically shielded cysteines. Repeat domains containing detected cysteines were represented as helical wheels. (*A*) Helices are viewed from the N terminus and show left-handed connectivity. Helices A, B, and C are the first, second, and third helix of the repeat domain, respectively. Arrows point from the N-terminal end to the C-terminal end of the helix. Heptad positions are labeled "a" to "g." Positions "a" and "d" are considered shielded from the aqueous environment. Positions "e" and "g" often participate in interhelix associations are defined as partially buried (2). Amino acids in linkers connecting helices are not shown. (*B–J*) Helical wheels of repeat domains. Heptad assignment was made according to sequence alignment with PDB ID codes 1CUN, 1S35, or 3E57 (*SI Materials and Methods*). Detected cysteines are colored yellow.

Fig. S2. Spectrin mouse and human sequence alignments. Domain sequences in mouse spectrin were aligned to sequences of existing crystal structures (see *SI Materials and Methods*), and the alignments shown to compare the location of detected cysteines to other functionally important amino acids or previously detected cysteines. In all alignments, detected cysteines are highlighted in yellow. Below each sequence, identical, conserved, and semiconserved amino acids are indicated by asterisks, colons, and periods, respectively. (*A*) The cysteine in the helical linker between β-spectrin repeats 8–9 has been previously detected (1). In this alignment, the helices of repeats 8 and 9 have been highlighted in cyan and light green, respectively, with the positions of "a" and "d" amino acids labeled above. The helical linker connecting repeats are shown in magenta, and the mouse and human forms differ by one amino acid. (*B*) The actin binding domain of mouse spectrin was aligned to that of human alpha-actinin1 to compare the location of Cys β112 of amino acids known to interact with actin. The helices of the CH1 and CH2 domains are highlighted in red and cyan, respectively, with their a–g identity labeled above. Amino acids in light green are surface exposed and believed to directly participate in the interaction with actin. The detected cysteine is within helix "e" of CH1, and its position on the helix shows that it is not of the same face as surface exposed amino acids and is probably not within the spectrin–actin interface. (*C*) Mouse and human β-spectrin repeats 13–15 were aligned to compare the location of Cys β1883 to ankyrin binding amino acids (cyan). The helices of repeats 13, 14, and 15 are highlighted in light green, red, and teal, respectively. The helical linker between repeats 13 and 14 is highlighted in light gray. The helical linker represents a stuttering in the a–g heptad ordering that occurs between repeats 13 and 14. According to the crystal structures for human repeats 14–15, such a stuttering does not occur between those repeats. The detected cysteine was distally located from ankyrin binding amino acids; however, it is possible that structural perturbations distal from the ankyrin binding site can affect spectrin–ankyrin interaction, as demonstrated by the locations of mutation sites previously found to destabilize spectrin–ankyrin binding (magenta).

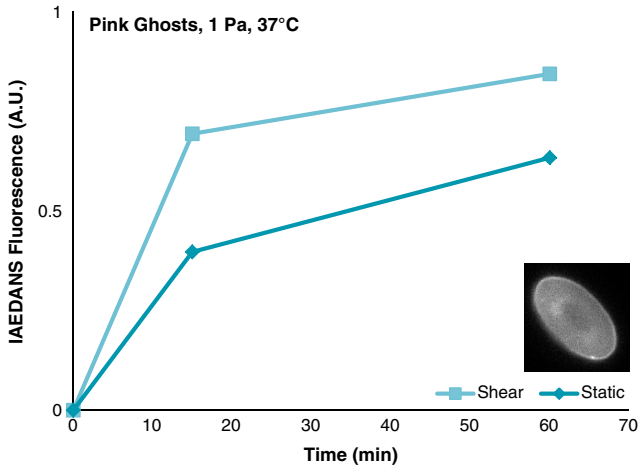

Fig. S3. Accelerated Cys labeling of spectrin in Wagner erythrocytes. Human Wagner erythrocytes containing spectrin with a currently uncharacterized mutation were generously provided by the Saad group (State University of Campinas). IAEDANS-labeled Wagner ghost reveals elliptocyte morphology characteristic of spectrin mutations. After normalizing IAEDANS fluorescence by Coomassie intensity, $\Phi_{15'} \approx 1.7$ and $\Phi_{60'} \approx 1.3$. The latter is closer to the result determined for 4.1R null cells in Fig. 2*C*.

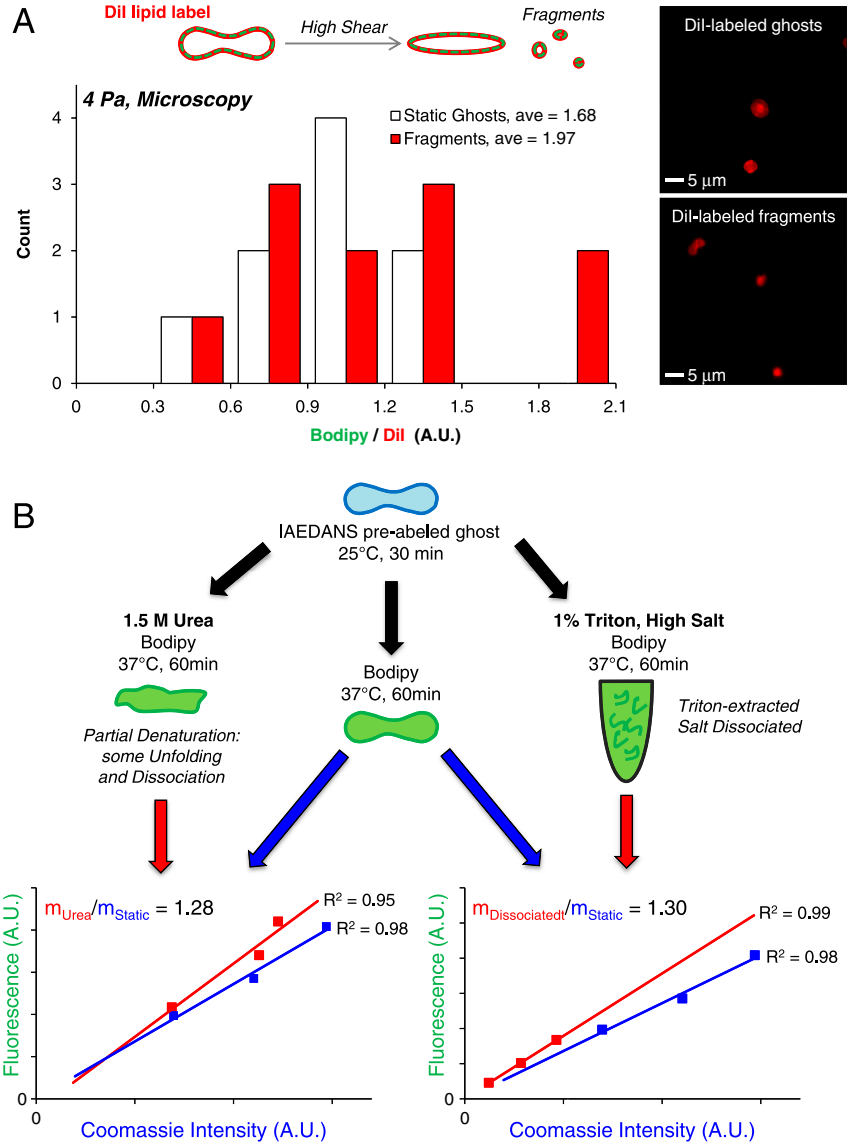

Fig. S4. Spectrin dissociation from binding partners increases cysteine labeling. Although network rupture ultimately removes stress on spectrin, immediately before rupture occurs, the spectrin network is extremely stressed, resulting in an increase in cysteine labeling. To show this, BODIPY labeling of fragments from stress-ruptured ghosts was compared to labeling of intact static-labeled ghosts (*Materials and Methods*). (*A*) Shearing at 4 Pa for 60 min creates fragments detectable by DiI. A histogram of BODIPY/DiI ratios, normalized to average BODIPY/DiI for static ghosts, shows increase variation of values for fragments. Although analysis is complicated by loss of spectrin in fragments, average BODIPY fluorescence, normalized by DiI intensity, approximately 17% greater for fragments than for whole ghosts. (*B*) After rupture, decrease in stress-induced unfolding is accompanied by exposure of cysteines ordinarily shielded by quaternary association. Ghosts were static labeled with BODIPY in PBS, 1.5 M urea, and 300 mM NaCl (*Materials and Methods*) to assess spectrin labeling in a network, under denatured conditions, and in a solubilized form. As previously shown (1), urea denaturation increases cysteine labeling. Under Triton-extracted, high salt conditions, spectrin is completely solubilized. Cysteines hydrophobically buried in repeat domains are shielded from solution while cysteines in binding sites are exposed to thiol probe, resulting in 30% greater labeling.

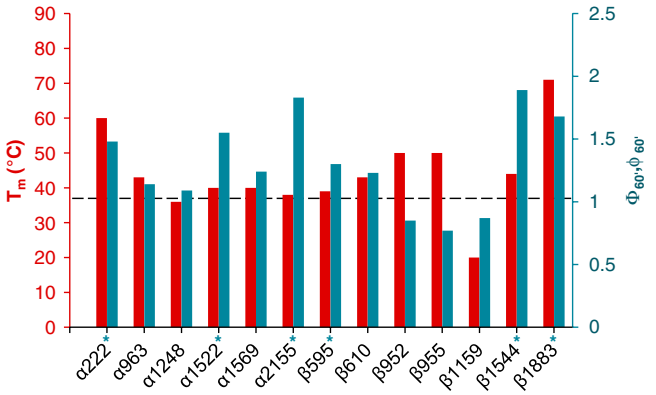

Fig. S5. T_M of human spectrin repeat domains compared with mouse spectrin $\Phi_{60'}$, $\varphi_{60'}$ Melting temperatures of individual repeat domains (1) were compared to $\Phi_{60'}$, $\varphi_{60'}$ values shown in Table S1. Blue asterisks correspond to blue stars in Fig. 5.

1. An X, Lecomte MC, Chasis JA, Mohandas N, Gratzer W (2002) Shear-response of the spectrin dimer-tetramer equilibrium in the red blood cell membrane. *J Biol Chem* 277:31796–31800.

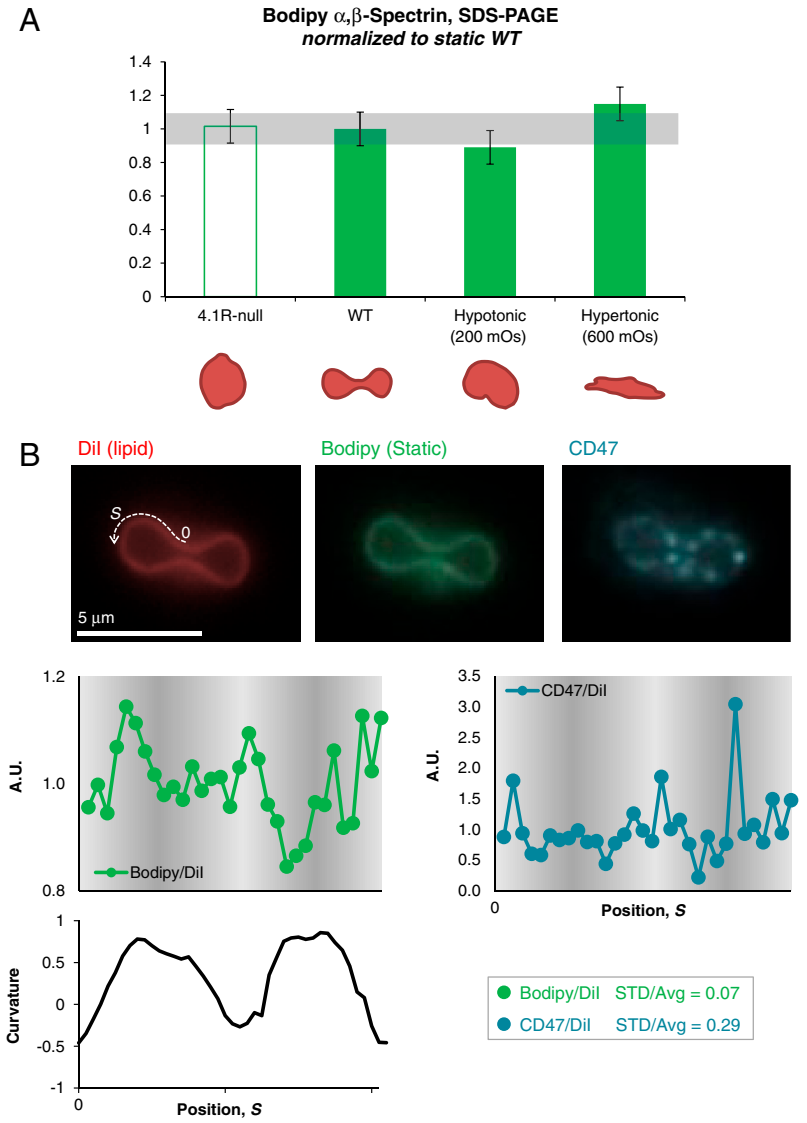

Fig. S6. Curvature effects on cysteine labeling. (*A*) 4.1R-null and wild-type RBC were static-labeled with two dyes under isotonic, hypotonic, and hypertonic buffers demonstrate the effects of curvature on spectrin labeling. IAEDANS prelabeled ghosts (blue) were split and incubated with BODIPY dye (green) under different osmotic conditions then subjected to SDS-PAGE analysis for spectrin (*Materials and Methods*). Ghosts in hypotonic buffer have less curvature and more closely resemble 4.1R-null ghosts in isotonic buffer, whereas ghosts in hypertonic buffer are flatter with some regions of high curvature, and yet spectrin labeling is not significantly different (within 10%). (*B*) BODIPY labeling along the membrane, normalized by DiI fluorescence in a side view of a ghost statically labeled in isotonic buffer shows that there is little variation in BODIPY labeling and again little correlation with membrane curvature. This is in contrast to CD47, which shows a high degree of variation along the membrane (note scale of graph and mean deviation) as we reported previously (1).

1. Subramanian et al. (2006) Membrane mobility and clustering of Integrin Associated Protein (IAP, CD47)—major differences between mouse and man and implications for signaling. *Blood Cell Mol Dis* 36:364–372.

Table S1. Rate constants from force-dependent Linderstrom–Lang fits of wild-type and 4.1R-null ghosts

Sample	$k_{1f}(\text{min}^{-1})$	$k_{1r}(\text{min}^{-1})$	R^2
WT, white ghosts	0.04	0.27	0.98
4.1-null, white ghosts	0.02	0	0.76

SDS-PAGE data was fit for k_{1f} and k_{1r} using the force-dependent Linderstrom–Lang equation previously described (1). Values for Δx and $\Delta x'$ were derived from previous single molecule experiments on spectrin repeats and have not changed from our earlier Cys labeling of human RBC. Shear area was reduced in proportion to the decrease in mouse to human red cell surface area. Parameter $k_2[\text{dye}] = 0.13\ \text{min}^{-1}$ as was determined from these earlier studies and held constant for wild-type and 4.1-null fits. Note that the zero time point in Fig. 2*C* reflects real data with error. The mechanical fragility was hypothesized to be due to a weakened spectrin–actin interaction, which is also reflected in the lower unfolding rate for 4.1R-null spectrin. If this dissociation occurs, cysteines in 4.1R null spectrin are not exposed due to force-induced unfolding but rather thermal fluctuations. For pink ghosts, $k_2[\text{dye}]$ was decreased to $0.085\ \text{min}^{-1}$, assuming k_{1f} and k_{1r} do not change from wild-type white ghosts parameters. Given the higher concentration of hemoglobin in pink compared to white ghosts, a lower effective labeling rate is expected.

Table S2. Cys-labeling ratios for spectrin peptides quantified by mass spectrometry

				IAEDANS		mBBr	
Peptide	Cys	Domain	Predicted accessibility	$\Phi_{30'}$	$\Phi_{60'}$	$\varphi_{30'}$	$\varphi_{60'}$
FYQYSQECEDILEWVK	α165	ABD	—			0.93	0.80
VNQYANECAQEK	α222	R3	partially buried	1.04	1.50	0.86	1.48
QCLDFHLFYR	α473	linker	—	1.43	1.60		
DQAEVCQQQQAAPVDEAGR	α963	R10	—			0.88	1.14
LCESHPDATEDLQK	α1248	R12	buried			0.88	1.09
DLEDLEEWINEMLPIACDESYK (4–5%)	α1522	R15	buried			1.32	2.43
DLEDLEEWINEMLPIACDESYKDPTNIQR						1.16	1.55
VCDGDEENMQEQLDK	α1569	R15B,Clinker	exposed	1.26	1.26	1.02	1.24
RVCDGDEENMQEQLDK (5–37%)				1.04	1.69	0.96	1.88
VQDVCAQGEDILNK	α1877	R18	buried			0.98	1.34
VQDVCAQGEDILNKEETQNK (30–41%)						1.17	1.45
NFEMCQEFEQNASAFLQWIQETR	α2155	R21	exposed	2.12	3.88	1.13	1.83
IHCLENVDK	β112	CH 1	—	0.76	1.83		
GYQPCDPQVIQDR	β595	R3B,Clinker	exposed	0.90	1.56	0.80	1.30
VSHLEQCFSELSNMAAGR	β610	R4	partially buried	1.22	1.67	1.02	1.23
VNNYCVDCEETSK	β952	R7	partially buried	0.76	1.23	0.84	0.85
$VNNYC_{mbbr}VDC_{mbbr}EETSK$	β955	R7	buried			0.57	0.77
$VNNYC_{IAEDANS}VDC_{mbbr}EETSK$						0.57	0.87
GNTLTQCLGFQEFQK	β1159	linker	—			0.99	0.87
AAEIDCQDIEER	β1544	R12	buried	0.90	1.46	0.81	1.89
EQEVSAAWQALLDACAGR	β1883	R15	buried	1.86	2.13	1.52	1.68

WT ghosts were prelabeled with IAEDANS under static conditions at room temperature for 30 min and then labeled with both IAEDANS and mBBr under shear conditions for 30 or 60 min. The Cys peptides detected by MS are listed together with amino acid number, spectrin domain, and predicted accessibility within the domain. Φ_{time} and φ_{time} are the ion-flux ratios of IAEDANS/IAM and mBBr/IAM Cys peptides, respectively, and are a measure of the force-enhanced labeling for individual cysteines (see Table S3 for raw data). Φ_{time} or φ_{time} values in bold indicate ion-flux ratios ≥ 1.25, which we define as force-enhanced labeling in Fig. 4. In cases of multiple peptides or labeling states, peptides with the greater ion flux were given preference (see Table S3). Cys β955 presents a special case, where the close proximity of Cys β952 and β955 results in multiple labeled states for a single peptide. The φ_{time} values for $VNNYC_{mbbr}VDC_{mbbr}EETSK$ are the ratios of the double mBBr labeled peptide to the completely unmodified peptide. $VNNYC_{IAEDANS}VDC_{mbbr}EETSK$ φ_{time} values represent the ratios of that peptide to the completely unmodified peptide. This peptide in the double IAEDANS labeled form was not detected. Nor were peptides with only Cys β955 modifiations. In this study these cysteines were classified as force-independently labeled, and further kinetic mass spectrometry studies are needed to clarify this complex behavior

Table S3. Ion-flux data of mass-spectometry detected peptides, α,β-spectrin

Peptide	Cys	$ST_{30'}$	$SH_{30'}$	$ST_{60'}$	$SH_{60'}$
FYQYSQEC$_{[IAM]}$EDILEWVK	α165	1.07E + 09	8.42E + 08	1.28E + 09	8.17E + 08
FYQYSQEC$_{[IAEDANS]}$EDILEWVK		2.81E + 07	2.06E + 07	4.05E + 07	2.06E + 07
VNQYANEC$_{[IAM]}$AQEK	α222	5.24E + 08	5.47E + 08	7.83E + 08	4.84E + 08
VNQYANEC$_{[IAEDANS]}$AQEK		1.14E + 07	1.24E + 07	1.60E + 07	1.48E + 07
VNQYANEC$_{[mBBr]}$AQEK		6.71E + 08	6.02E + 08	6.86E + 08	6.27E + 08
QC$_{[IAM]}$LDFHLFYR	α473	9.62E + 06	8.32E + 06	1.83E + 07	1.10E + 07
QC$_{[IAEDANS]}$LDFHLFYR		2.71E + 07	3.35E + 07	3.44E + 07	3.30E + 07
DQAEVC$_{[IAM]}$QQQQAAPVDEAGR	α963	3.69E + 08	3.63E + 08	5.15E + 08	3.53E + 08
DQAEVC$_{[mBBr]}$QQQQAAPVDEAGR		1.87E + 09	1.61E + 09	2.26E + 09	1.77E + 09
LC$_{[IAM]}$ESHPDATEDLQK	α1248	2.72E + 08	2.70E + 08	3.51E + 08	2.71E + 08
LC$_{[IAEDANS]}$ESHPDATEDLQK		9.71E + 08	8.75E + 08	1.33E + 09	1.05E + 09
LC$_{[mBBr]}$ESHPDATEDLQK		6.19E + 08	5.42E + 08	7.52E + 08	6.30E + 08
DLEDLEEWINEMLPIAC$_{[IAM]}$DESYK (4%)	α1522	1.78E + 07	1.58E + 07	1.99E + 07	1.82E + 07
DLEDLEEWINEMLPIAC$_{[mBBr]}$DESYK (3–5%)		1.86E + 07	2.38E + 07	1.14E + 07	2.34E + 07
DLEDLEEWINEMLPIAC$_{[IAM]}$DESYKDPTNIQR		3.81E + 08	3.69E + 08	5.00E + 08	4.22E + 08
DLEDLEEWINEMLPIAC$_{[mBBr]}$DESYKDPTNIQR		3.99E + 08	4.48E + 08	3.20E + 08	4.21E + 08
VC$_{[IAM]}$DGDEENMQEQLDK	α1569	8.74E + 07	6.74E + 07	1.12E + 08	7.62E + 07
VC$_{[IAEDANS]}$DGDEENMQEQLDK		1.04E + 08	1.01E + 08	1.62E + 08	1.39E + 08
VC$_{[mBBr]}$DGDEENMQEQLDK		1.29E + 09	1.02E + 09	1.54E + 09	1.30E + 09
RVC$_{[IAM]}$DGDEENMQEQLDK (20–27%)		2.14E + 07	2.26E + 07	4.04E + 07	1.92E + 07
RVC$_{[IAEDANS]}$DGDEENMQEQLDK (32–37%)		5.42E + 07	5.93E + 07	8.23E + 07	6.56E + 07
RVC$_{[mBBr]}$DGDEENMQEQLDK (5–6%)		6.45E + 07	6.53E + 07	8.00E + 07	7.14E + 07
VQDVC$_{[IAM]}$AQGEDILNK	α1877	1.83E + 09	1.45E + 09	2.58E + 09	1.50E + 09
VQDVC$_{[mBBr]}$AQGEDILNK		1.62E + 08	1.26E + 08	1.59E + 08	1.24E + 08
VQDVC$_{[IAM]}$AQGEDILNKEETQNK (30–34%)		7.81E + 08	7.38E + 08	1.13E + 09	6.70E + 08
VQDVC$_{[mBBr]}$AQGEDILNKEETQNK (38–41%)		1.01E + 08	1.11E + 08	1.00E + 08	8.60E + 07
NFEMC$_{[IAM]}$QEFEQNASAFLQWIQETR	α2155	2.53E + 07	2.33E + 07	3.72E + 07	3.07E + 07
NFEMC$_{[IAEDANS]}$QEFEQNASAFLQWIQETR		2.05E + 06	3.99E + 06	9.85E + 05	3.16E + 06
NFEMC$_{[mBBr]}$QEFEQNASAFLQWIQETR		3.80E + 08	3.94E + 08	2.92E + 08	4.41E + 08
IHC$_{[IAM]}$LENVDK	β112	1.19E + 08	9.31E + 07	2.64E + 08	1.77E + 08
IHC$_{[IAEDANS]}$LENVDK		3.58E + 08	2.13E + 08	3.27E + 08	4.00E + 08
GYQPC$_{[IAM]}$DPQVIQDR	β595	8.09E + 07	5.56E + 07	1.47E + 08	1.05E + 08
GYQPC$_{[IAEDANS]}$DPQVIQDR		2.20E + 08	1.36E + 08	2.00E + 08	2.28E + 08
GYQPC$_{[mbbr]}$DPQVIQDR		1.98E + 09	1.09E + 09	2.37E + 09	2.14E + 09
VSHLEQC$_{[IAM]}$FSELSNMAAGR	β610	3.68E + 08	2.32E + 08	6.38E + 08	4.84E + 08
VSHLEQC$_{[IAEDANS]}$FSELSNMAAGR		2.84E + 07	2.19E + 07	2.52E + 07	3.19E + 07
VSHLEQC$_{[mbbr]}$FSELSNMAAGR		1.11E + 09	7.16E + 08	1.30E + 09	1.25E + 09
VNNYC$_{[IAM]}$VDC$_{[IAM]}$EETSK (5–6%)	β952	1.79E + 07	1.32E + 07	3.79E + 07	2.96E + 07
VNNYC$_{[IAEDANS]}$VDC$_{[IAM]}$EETSK (11–15%)		5.58E + 07	3.13E + 07	7.15E + 07	6.86E + 07
VNNYC$_{[mbbr]}$VDC$_{[IAM]}$EETSK		2.93E + 08	1.81E + 08	5.42E + 08	3.58E + 08
VNNYC$_{[mbbr]}$VDC$_{[mbbr]}$EETSK	β955	5.52E + 07	2.32E + 07	6.98E + 07	4.19E + 07
VNNYC$_{[IAEDANS]}$VDC$_{[mbbr]}$EETSK (22–28%)		2.14E + 07	8.96E + 06	1.93E + 07	1.31E + 07
GNTLTQC$_{[IAM]}$LGFQEFQK	β1159	3.72E + 08	2.33E + 08	4.99E + 08	4.90E + 08
GNTLTQC$_{[mbbr]}$LGFQEFQK		1.61E + 09	9.98E + 08	1.98E + 09	1.69E + 09
AAEIDC$_{[IAM]}$QDIEER	β1544	8.59E + 07	5.75E + 07	1.59E + 08	1.26E + 08
AAEIDC$_{[IAEDANS]}$QDIEER		5.77E + 08	3.47E + 08	5.14E + 08	5.96E + 08
AAEIDC$_{[mbbr]}$QDIEER		2.01E + 09	1.09E + 09	2.22E + 09	2.09E + 09
EQEVSAAWQALLDAC$_{[IAM]}$AGR	β1883	1.62E + 07	8.13E + 06	4.62E + 07	2.86E + 07
EQEVSAAWQALLDAC$_{[IAEDANS]}$AGR		3.39E + 08	3.17E + 08	2.83E + 08	3.72E + 08
EQEVSAAWQALLDAC$_{[mbbr]}$AGR		9.50E + 08	7.26E + 08	9.75E + 08	1.01E + 09

Ion-flux data of mass-spectometry detected peptides. The raw mass spectrometry ion-flux data Φ_{time} and φ_{time} were calculated from the ratio of IAM and mBBr/IAEDANS peptides in (**A**) α-spectrin and (**B**) β-spectrin. When multiple peptides for the same cysteine were detected, peptides with the greater ion-flux values (bold) were used for analysis. In a majority of cases, less abundant peptides make up less than a third of the total pool.

Table S4. Cys-labeling ratios for ankyrin peptides quantified by mass spectrometry

Peptide	Cys	Repeat	$\Phi_{30'}$	$\Phi_{60'}$	$\varphi_{30'}$	$\varphi_{60'}$
TKDELTPLHCAAR	274	R8	0.88	1.56	0.67	1.26
NGLSPIHMAAQGDHLDC$_{mBBr}$VR (100%)	316	R9	—	—	—	—
AKDDQTPLHC$_{IAEDANS}$AR (100%)	472	R14	—	—	—	—
LCQDYDTIGPEGGSLR	1022	N/A	—	—	1.61	1.76
FWLSDCPR (100% IAM)	1212	N/A	—	—	—	—

The detected Cys peptides for ankyrin are listed together with amino acid number (according to Uniprot accession no. Q02357), repeat, Φ_{time} and φ_{time} (modified/unmodified ion-flux ratios for IAEDANS and mBBr). Ankryrin repeats consist of two alpha helices separated by β-loop turns, and the borders for ankyrin repeats were defined according to Uniprot entry Q02357. Although spectrin repeats fold into independent, protease resistant structures (1), the same cannot be said for ankyrin repeats, despite their labeling as individual domains. Three cysteines, Cys 316 and 472 were only detected in the modified form; therefore Φ_{time} and φ_{time} were not calculated for these peptides. The modification is listed in the peptide sequence, Cys-274-IAEDANS and Cys-472-mBBr were not detected. Cys 1212 was only detected in the unmodified form, and the zero Φ_{time} and φ_{time} values shown as dashes.

1. Kahana E, Marsh PJ, Henry AJ, Way M, Gratzer WB (1994) Conformation and phasing of dystrophin structural repeats. *J Mol Biol* 235:1271–7.